Towards a compact and low-cost mesoscopic XY positioning system using 3D printing of conductive polymers

Benjamin Calmé[1,2], Lennart Rubbert[2] and Yassine Haddab[1]

***Abstract*— Technological advances in additive manufacturing have made it possible to exploit composite materials, such as carbon-doped filaments, synthesised for specific function with tailored properties. The integration of carbon fibres, with good electrical and thermal conductivity, within an insulating polylactic acid (PLA) matrix produces a conductive functional material. These properties allow to manufacture mesoscopic electrothermal actuators and more complex monolithic structures including them.**

A compact and monolithic 3D printable positioning system with built-in V-shaped actuators is proposed in this paper. Multi-physics coupling analysis are performed in ANSYS to validate the estimated performances of the actuator and the positioning system. Then, an experimental characterisation based on printed prototypes showed good performances close to those estimated. The prototype measures 92mm×92mm×2mm and has a working space of 10.75mm^2. These early results allowed the implementation of a first closed-loop control strategy using a Smith predictor.

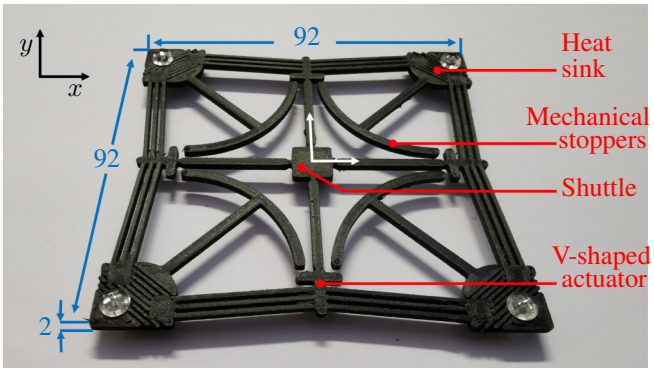

Fig. 1: Structure of the 3D-printed monolithic 2D positioning system (unit: mm).

I. INTRODUCTION

Miniaturisation proved to be of great importance in several areas of mechatronics, such as medical robotics or space applications. Technological advances in these fields have made it possible to produce smaller, more compact and therefore more portable devices [1], [2]. However, this scaling down is more complex for traditional actuators and is associated with a difficult assembly phase. The miniaturisation of traditional devices such as electric motors, pneumatic and hydraulic actuators comes at the cost of a significant decrease in performance. Thus, in mesorobotics and microbotics, actuators of various kinds tend to replace traditional actuation technologies [3]. These include thermomechanical actuators [4], some of which can be regarded as flexible mechanisms. U-shaped [3], V-shaped and Z-shaped actuators [5] are the three main electrothermal flexible actuators able to produce planar displacements. This is a clear advantage when designing compliant structures with built-in actuators [6], [7]. In addition to being scalable and monolithic, flexible mechanisms have many advantages in terms of accuracy and repeatability due to the avoidance of wear and mechanical play because of the absence of contact and therefore friction.

The technological development of manufacturing methods, such as additive manufacturing, and the research for new types of materials have led to more freedom in design. Composite materials, such as carbon-doped PLA, obtained by infusing carbon fibres into a polymer matrix, have resulted in a functional material with improved mechanical behaviour and new physical properties [8]. Carbon fibres are particularly known in engineering for their good mechanical characteristics due to their crystalline structure. They also have good conductive properties due to the sp^2 hybridisation of the carbon atoms. The initially insulating polymer becomes, for a minimal inclusion of carbon fibres, a conductive composite material. The characterisation of such materials and their electrothermal properties is a hot topic of research [8]. The design of actuators based on doped material, e.g. carbon doped resin, using Joule effect and thermal expansion have already been investigated [9].

The contribution of this paper is to propose a compact 2D positioning system (17cm^3) with built-in actuators. The originality of the design proposed in this paper lies in the use of the freedom offered by 3D printing to be able to manufacture in a monolithic way the positioning platform, the four independent actuators and the cooling system. The system is therefore ready to be used, low-cost and can be manufactured with the majority of PLA-compatible 3D printers, as shown in Fig. 1. It is also provided the first elements of an easily usable closed loop control strategy.

The paper is organised as follows. In Section II, the design concepts and the analytical models are introduced and validated with finite element analysis. In Section III, the experimental characterisation is presented as well as the base of the control strategy. Conclusions are given in Section IV.

[1]Benjamin Calmé and Yassine Haddab are with LIRMM, University of Montpellier, CNRS, Montpellier, France. benjamin.calme@lirmm.fr

[2]Benjamin Calmé and Lennart Rubbert are with ICube, University of Strasbourg, France.

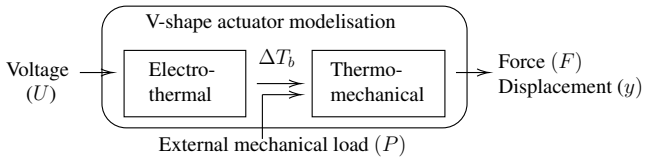

Fig. 2: Schematic representation of the analytical modelling of the actuator

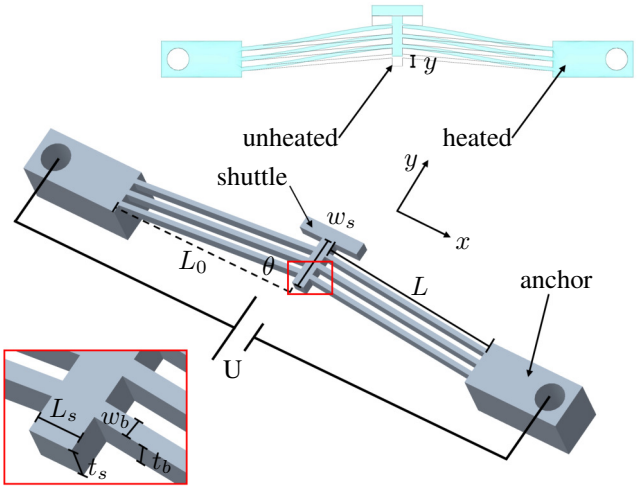

Fig. 3: CAD model illustration of the V-shaped electrothermal actuator and parameter identification.

II. ELECTROTHERMAL ACTUATOR MODELLING

In order to build a 2D positioning system, V-shaped actuators will be used. Z-shaped actuators showed poorer performance in terms of output force and motion [5], and since rectilinear motion is expected, U-shaped actuators are excluded. The V-shaped actuator consists of two beams, inclined at an angle of θ, fixed to a central shuttle on one end and an anchor on the other.

A. V-shape actuator analytical model

The design and functioning of this actuator are based on the use of carbon fibres in the PLA. When a voltage is applied to the actuator, the natural electrical resistance induces Joule heating. The temperature generated leads to thermal expansion, symmetrically varying the length of the beams and thus causing the displacement of the central shuttle y. Consequently, the analytical modelling of this type of actuator is done in two steps, a first step to model the electrothermal effect and a second step to model the thermomechanical effect, as shown in Fig. 2.

1) Electrothermal Model: When a voltage is applied, the heat generated by the Joule effect is dissipated simultaneously by radiation and convection until a steady state thermal equilibrium is reached. Both of this thermal mechanisms can be neglected at first with small scale actuator. According to [10], the average temperature increase along the beams ΔT_b

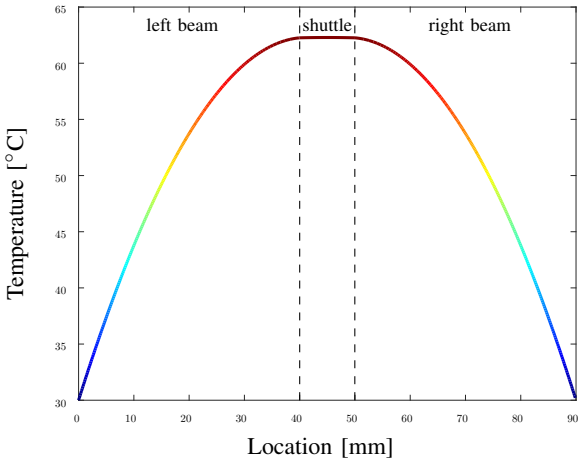

Fig. 4: Temperature distribution within the actuator based on the analytical model

is established as function of the input voltage U, geometrical parameters of the beam Π and the material properties Q as follows:

$$\Delta T_b = \frac{1}{L}\int_0^L (T_s - T_0) = Q\Pi U^2 \tag{1}$$

with,

$$Q = \frac{1}{k_a \rho}, \quad \Pi = \frac{\left(1 - e^{L\Gamma}\right)^2}{Le^{L\Gamma}\Gamma}\varphi + \left(\frac{1 - e^{L\Gamma}}{Le^{L\Gamma}\Gamma} + 1\right)\chi \tag{2}$$

where $\Gamma = \sqrt{k_a/(kt_b)}$, L is the beam length, k_a is the thermal conductivity of the air, k is the thermal conductivity of beam, ρ is the electric resistivity. The calculation details of φ and χ, which are depending on the geometrical parameters, shown in Fig. 3, are clearly presented in [10].
In Fig. 4, the temperature distributions along the actuator, analytically calculated, is given for $U = 50V$. The shuttle has the highest temperature due to its greater resistivity. The temperature of 60 degrees is the limit for PLA before glass transition. Exceeding this glass transition temperature will result in a change in the behaviour of the material, which will tend to a plastic deformation.

2) Thermomechanical Model: According to [10], considering the symmetry of the actuator and the shuttle as infinitely rigid and not subject to thermal expansion, then the shuttle displacement is obtained from the following Castigliano theorem:

$$y = \Delta L_T \sin\theta - \int_0^L \frac{N}{EA_b}\frac{\partial N}{\partial P}dx - \int_0^L \frac{M}{EA_b}\frac{\partial M}{\partial P}dx \tag{3}$$

where ΔL_T is the axial elongation of the beam linked to thermal expansion, θ is the inclination angle of the beam. M and N are the bending moment and the axial force on the beam. E is the Young's modulus of the beam material. This equation can be simplified by substituting boundary conditions, such as

$$y = \begin{pmatrix} \alpha L\Phi \sin\theta & -L\dfrac{\Phi}{EA_b} \end{pmatrix} \begin{pmatrix} \Delta T_b \\ P \end{pmatrix}, \tag{4}$$

where α is the coefficient of thermal expansion and $\Phi = L_0^2/(h_0^2\cos^4\theta + L_0^2\sin^2\theta)$. L_0 is the distance between the two anchor points of the beam. The elements of the left-hand side of Eq. (4) thus represent the flexibility of the actuator in response to the temperature and in response to an external load P. The load P will be the spring force of the actuator mounted in opposition in the case of the positioning system, as shown in Fig. 5.

3) Combined actuator models: By combining the two models, Eq. (4) can be rewritten as follows :

$$y = \begin{pmatrix} \alpha L_0 \Gamma \sin\theta QT & -\dfrac{L_0\Gamma}{EA_b cos\theta} \end{pmatrix} \begin{pmatrix} U^2 \\ P \end{pmatrix} \tag{5}$$

$$= (\kappa_1 - \kappa_2) \begin{pmatrix} U^2 \\ P \end{pmatrix} \tag{6}$$

By modelling the force related to an input voltage as a spring pushing the shuttle, the equation for the force F produced by the actuator can be established as follows [10]:

$$F = \xi U^2 - P \quad \text{with} \quad \xi = \frac{\kappa_1}{\kappa_2} \tag{7}$$

B. Modelling the 2D positioning system

1) Voltage distribution in the monolithic structure: In order to produce the 2D positioning system, the insulation of the part between the different actuators must be done. The first approach is only relevant for certain category of 3D printers, able to extrude different materials during the same printing process. This option offers the opportunity to print the entire platform as a single rigid piece by connecting the actuators, printed in carbon PLA, with an electrically insulating polymer, as shown in Fig. 6a.
The main contribution is done in the other case, in order to make it compatible with the largest number of printers, the phenomena of electrical and thermal conduction in the design have to be considered, as shown in Fig. 6d. The first step is to model the mechanism as a series of resistors. A perfect electrical insulator has infinite resistance, which can be expressed in the design, according to Fig. 5, as $R_2 \gg R_1$. In order to increase the resistance, the length and resistivity have to be maximised and the cross-section has to be minimised, according to the following equation:

$$R = \rho\frac{l}{s} \tag{8}$$

The first aspect to consider is that although the material has become conductive due to the carbon, it retains a high electrical resistivity. Then, the conductive properties of the printed material are dependent of the orientation of the neutral fibres, which is defined by the direction of movement of the nozzle. According to [11], an 100% infill pattern with lines was then chosen to maximise the electrical resistivity.

During the design process, the application of a simple pattern allowed the cross-section to be reduced by exploiting the smallest printing parameters allowed by the printer. The pattern to reduce the cross-sectional area was also chosen to exploit the laminar flow cooling properties of the heat sinks and thus avoid heat conduction to the adjacent actuators.

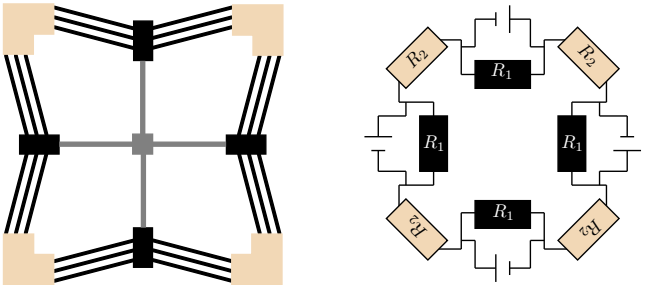

Fig. 5: Electrical representation based on a resistor set equivalent to the monolithic positioning system.

2) Actuation against opposite actuators: The actuators are in opposition two by two. When one is actuated, the other is loaded and must deform. It is therefore necessary to calculate the force-displacement relationship of the actuator at rest when it is loaded. This quantity allows us to know the minimum force F that the active actuator must provide to deform the one at rest. The force-displacement characteristic curve of this pre-shaped mechanism has two domains. A linear domain in which the evolution of the force f, is calculated as follows [12]:

$$f = 64\pi^2 \frac{EIL\sin\theta}{(2L)^3}\left(\frac{4}{3} - \frac{y}{L\sin\theta}\right) \tag{9}$$

And a non-linear domain where the relationship between the force f, the normalized axial force N and the deformation generated by the active actuator y is calculated according to [12], as follows:

$$f = \frac{EIL\sin\theta}{(2L)^3}\left(\frac{N^3}{\frac{N}{4} - \tan\frac{N}{4}}\right)\left(\frac{N^2}{N^2 - 4\pi^2} - \frac{y}{L\sin\theta}\right) \tag{10}$$

$$\frac{3}{16N^4}\left(1 + \frac{\tan^2(N/4)}{3} - \frac{\tan(N/4)}{(N/4)}\right)f^2 - \frac{4\pi^2}{(N^2-4\pi^2)^2}f + \frac{N^2}{12(L\sin\theta/w_b)^2} - \frac{N^2\pi^2(N^2-8\pi^2)}{4(N^2-4\pi^2)^2} = 0 \tag{11}$$

where I is the quadratic moment of the beam and $N = \sqrt{\mu(2L)^2/(EI)}$ with μ the axial force. The solution is given by a numerical method.

C. Finite element analysis

The multiphysics numerical simulation was performed with the ANSYS solver implemented in Creo Parametric 6.0. The analyses were conducted by coupling the electrical, thermal and mechanical fields. The geometrical parameters used are shown in Tab. I. The properties of the material used in the simulations are derived from an experimental characterisation phase as explained in Subsection III-A.

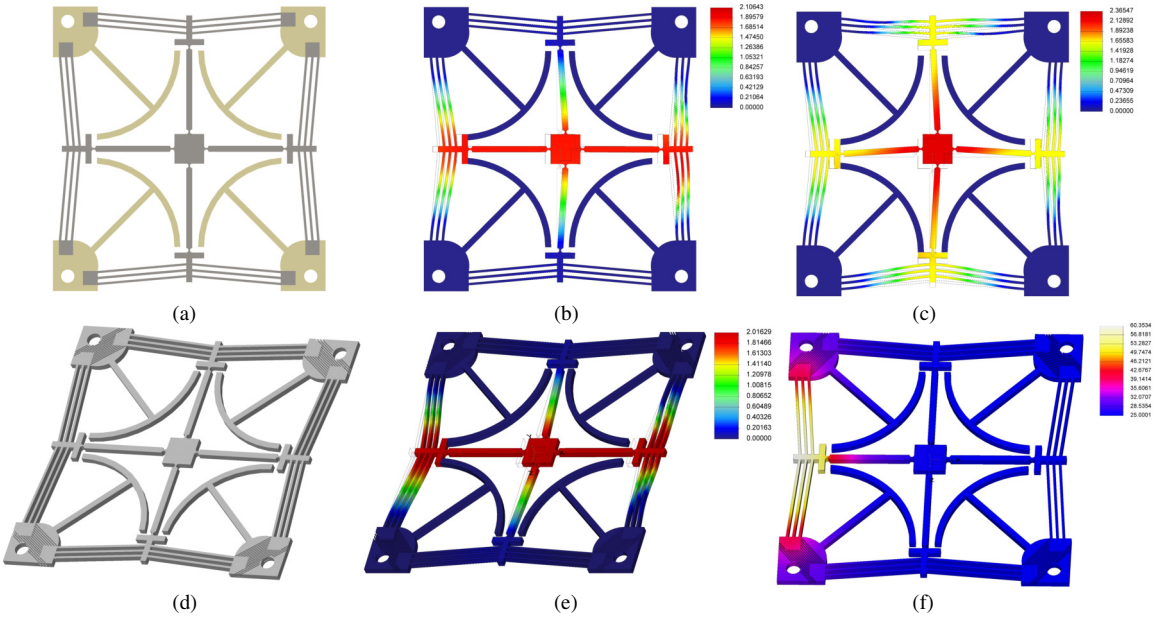

Fig. 6: Finite element simulation result for a 2D positioning system. (6a) represents the CAD of the positioning system manufactured in bi-material. (6b) and (6c) illustrate the simulation results obtained by FEA following the actuation of the left actuator and the left and bottom actuators. (6d) represents the CAD of the monolithic positioning system. (6e) and (6f) illustrate the thermomechanical and electrothermal FEA results of the same simulation, following the actuation of the left actuator with the monolithic positioning system. The sub-figures (6d)(6e)(6f) are illustrated in perspective in order to visualise the pattern used to increase the resistance of the sections between actuators.

TABLE I: Design parameters

Material parameters						
E [MPa]	E' [MPa]	R [Ohm]	R' [Ohm]	ρ [Ohm.m]	d [Kg.m^{-3}]	k [Wm^{-1}K^{-1}]
3300	3140	800-1200	900	0.06	1150	0.366
Geometric parameters						
L [mm]	θ	L_0 [mm]	t_s = t_b [mm]	w_s [mm]	w_b [mm]	L_s [mm]
30	5	29.89	2	8	0.8	2

The model is set to couple the multiphysics phenomena, while assuming constant materials properties. In other words, the electric current flowing through the actuator will heat the material, but the increase in temperature and deformation of the material will not affect the current. The non-linearity of these aspects will be integrated in future optimisation study. For the thermoelectric simulation a voltage was applied to the conductive material and thus simulate heat generation by Joule effect. The faces of the actuator are set to a convective heat boundary condition, simulating the air temperature around with the heat flux option.

The simulation results for the positioning system are shown in Fig. 6. Simulations have been carried out for a dual-material positioning system and for a single-material positioning system. Simulation results with one or two actuators operating simultaneously are presented Fig. 6b and Fig. 6c. The feasibility of the single-material mechanism is demonstrated by the sub-figures Fig. 6e and Fig. 6f corresponding to the same simulation, one for the mechanical aspect and the other for the thermal aspect.

The stroke of the mechanism is almost the same as for the mechanism with insulating material, which proves that the design does not affect the performance. The electro-thermal simulation shows that the temperature in the actuator, through which the current flows, does increase. It also shows that the temperature in the other actuators is not affected by the temperature variation of one. The actuators can therefore be controlled independently.

III. EXPERIMENTAL EVALUATION

A. Experimental characterisation of the material

The material used for these experiments is Original Carbon Fiber PLA (Proto Pasta). It was printed with an Ultimaker S3 at an extrusion temperature of 240°C degrees, at a speed of 30mm/s on a bed heated to 60°C.

Resistance R' was measured with an ohmmeter. The sample to be measured being placed between the probes of the ohmmeter. The resistivity ρ was then calculated according to Eq. (8). Electrical heating performance of the sample was determined based on surface temperature with various applied voltages while using a DC power supply. The range of applied voltage was from 20 to 50 V with 5 V intervals. As the contact could not be made by soldering, it was made by means of a screw-nut embedding. A K-type thermocouple was used to measure the surface temperature after applying different voltages.

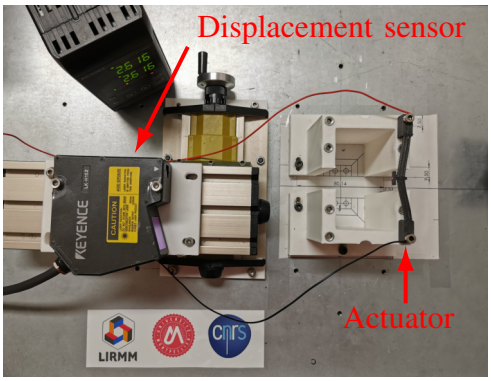

Fig. 7: Experimental set-up for the characterisation of the electro-thermal actuator

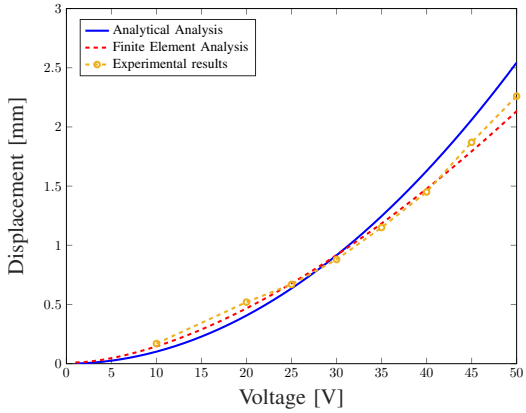

Fig. 8: Displacement obtained for the electrothermal actuator as a function of the input voltage.

The mechanical characterisation of the material was carried out with a FK50 force sensor (Sauter) and a LK-H152 laser-based displacement sensor (Keyence), as detailed in [13]. A beam was printed with carbon-PLA and the Young's modulus E' was characterised using Euler Bernoulli's relationship between applied force F and measured displacement δ:

$$E' = \frac{FL^3}{3\delta I} \tag{12}$$

where I the quadratic moment of the cross section and L the length of the beam. The characterized Young's modulus is 3140MPa, which is consistent with some earlier characterisation of the material [14].

B. Experimental characterisation of the V-shaped electrothermal actuator

The behaviour of the actuator was characterised experimentally by means of the experimental set-up shown in Fig. 7. The shuttle displacement was measured for different voltage values ranging from 10 to 50V in 5V steps and with a return to room temperature in between. The experimental results are presented in Fig. 8. The experimentally measured values are in good accordance with the results of previous models.

At 55V, the temperature of the measured actuator was $64°C$, i.e. beyond the glass transition phase indicated by the manufacturer. It is noted that after reaching this temperature, the actuator does not recover its initial configuration. The displacement sensor indicates a position of 0.13mm despite the mechanism returning to room temperature.

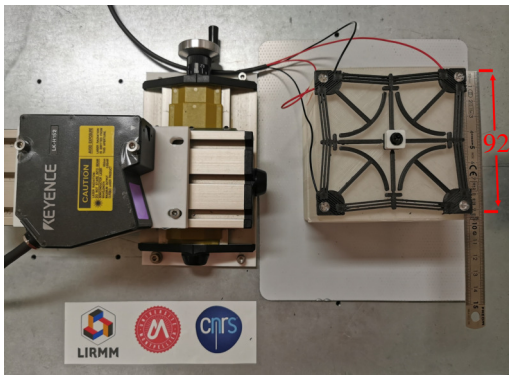

Fig. 9: Experimental setup of the XY positioning system (unit: mm).

TABLE II: Performance comparisons between the proposed positioning system and previous reported parallel stages

Ref	Actuator	Dimension [mm]	Motion range
[15]	piezoelectric	50x50x10	14,32x14,32 [μm]
[16]	electromagnetic	120x120x25	11,75x11,6 [mm]
Proposed	electrothermic	92x92x2	3,7x3,7 [mm]

C. Experimental characterisation of the positioning system

The performance of the positioning system has been analysed using the same equipment as before, as shown in Fig 9. After applying a voltage to one of the actuators, the displacement of the central shuttle was measured using the displacement sensor. By driving an actuator with a conservative voltage of 50V, an average motion range of 1.85mm is achieved. This also corresponds to a total motion range of 3.7mm along each axis. For a given desired position, the manipulator was operated 21 times with a open loop voltage of 40V. The average displacement measured was 1.32 mm and the standard deviation was 0.17 mm. An error of 17% is found between the actuator estimated and measured values. However, an error of only 4% is found between the measured and estimated force-displacement relationship with respect to the opposite actuator. In line with the fact that this is preliminary results with a 3D printed composite material, and therefore particularly non-linear, the error obtained seems acceptable. As presented in Tab. II, given the millimetre range of motion achieved, the objective of designing a compact and low-cost positioning system is successfully achieved. The presence of nonlinear effect requires the implementation of control strategy in order to achieve a precision positioning. The precepts are introduced in the following section.

D. Control strategy of the actuator

The temperature rise takes much longer than the temperature-position conversion time, which induces a large dead-time τ. The use of a PID would be limited since the time delay would enter the loop and considerably decrease

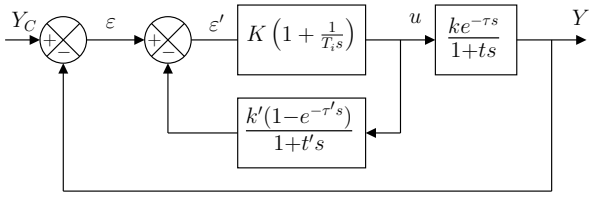

Fig. 10: Structure of Smith predictor based on PI control strategy

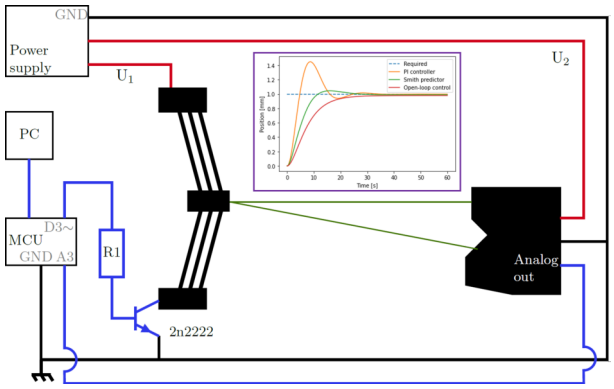

Fig. 11: Shematic of the experimental set-up used to validate the actuator control strategy and step response with open-loop control, PI controller and Smith Predictor.

the performance of the control. A Smith predictor is a predictive controller designed to control systems with a significant feedback delay and here proposed with a PI controller. The PI controller is therefore set for a process without delay and then a final controller for the process with delay is calculated from the previous one, as shown in Fig. 10. After prior identification of the process, $k' = k$, $\tau' = \tau$ and $t' = t$ are set to have a process modelled as a first order system. The validation of this control strategy was done using the set-up illustrated in Fig. 11, where a comparison of the experimental results of step responses of the system for the real-time control strategies is also given. In view of these results, this control strategy seems encouraging.

IV. CONCLUSIONS

In this article, the feasibility of manufacturing a monolithic positioning system with built-in thermoelectric actuators using 3D printers is presented. The consideration of electrical and material properties as a constant allows for voltage control (constant resistance) in the 10.75mm^2 workspace. In future work, we will be interested in integrating non-linearities and considering their variability in order to clearly defined the precision and stability of the prototype.

In this paper, an approach is proposed to specifically use doping (actuation and heat dissipation) by design. This approach shows the interest of controlling the doping and density of the conductive fibre in order to obtain precise performances to meet specific needs or constraints.

Two axes of research concerning the composite material are being studied in order to improve its performance. Although the chosen filament offers one of the lowest resistivities, this is still significant and could be improved by doping it with another type of material, such as copper. The nature of the matrix determines the conduction and thermal expansion properties. Acrylonitrile Butadiene Styrene (ABS) and PolyEthylene Terephthalate Glycol (PETG) have better characteristics than PLA and could offer better behaviour. Future work will focus on the self-sensing capabilities of this type of device and the possibility of using this positioning system for low-cost atomic force microscopes for schools.

ACKNOWLEDGMENT

This work was supported by the Investissements d'Avenir (Labex CAMI ANR-11-LABX-0004).

REFERENCES

[1] T. J. Teo, G. Yang, and I.-M. Chen, "Compliant Manipulators," Mar. 2014, pp. 1–64.

[2] H. Zhang, Z. Wu, and Q. Xu, "Design of a New XY Flexure Micropositioning Stage With a Large Hollow Platform," *Actuators*, vol. 9, no. 3, p. 65, Sept. 2020.

[3] H. Hussein, A. Tahhan, P. L. Moal, G. Bourbon, Y. Haddab, and P. Lutz, "Dynamic electro-thermo-mechanical modelling of a U-shaped electro-thermal actuator," *Journal of Micromechanics and Microengineering*, vol. 26, no. 2, Jan. 2016.

[4] A. Potekhina and C. Wang, "Review of Electrothermal Actuators and Applications," p. 28, 2019.

[5] Z. Zhang, Y. Yu, X. Liu, and X. Zhang, "Dynamic modelling and analysis of V- and Z-shaped electrothermal microactuators," *Microsystem Technologies*, vol. 23, no. 8, pp. 3775–3789, Aug. 2017.

[6] T. Moulton and G. K. Ananthasuresh, "Micromechanical Devices With Embedded Electro-Thermal-Compliant Actuation," Sens," *Actuators A*, pp. 38–48, 2001.

[7] K. Alblalaihid, J. Overton, S. Lawes, and P. Kinnell, "A 3D-printed polymer micro-gripper with self-defined electrical tracks and thermal actuator," *Journal of Micromechanics and Microengineering*, vol. 27, no. 4, Apr. 2017.

[8] H. Kim and S. Lee, "Characterization of Electrical Heating of Graphene/PLA Honeycomb Structure Composite Manufactured by CFDM 3D Printer," *Fashion and Textiles*, vol. 7, p. 8, Mar. 2020.

[9] O. Ulkir, "Design and fabrication of an electrothermal MEMS micro-actuator with 3D printing technology," *Materials Research Express*, vol. 7, no. 7, July 2020.

[10] Z. Zhang, W. Zhang, Q. Wu, Y. Yu, X. Liu, and X. Zhang, "Closed-form modelling and design analysis of V- and Z-shaped electrothermal microactuators," *J. Micromech. Microeng.*, p. 13, 2017.

[11] A. Dorigato, V. Moretti, S. Dul, S. H. Unterberger, and A. Pegoretti, "Electrically conductive nanocomposites for fused deposition modelling," *Synthetic Metals*, vol. 226, pp. 7–14, Apr. 2017.

[12] H. Hussein, P. Le Moal, G. Bourbon, Y. Haddab, and P. Lutz, "Modeling and Stress Analysis of a Pre-Shaped Curved Beam: Influence of High Modes of Buckling," *International Journal of Applied Mechanics*, vol. 07, no. 04, 2015.

[13] M. Ben Salem, G. Aiche, Y. Haddab, L. Rubbert, and P. Renaud, "Additive Manufacturing of a Bistable Mechanism Using Fused Deposition Modeling: Experimental and Theoretical Characterization," in *Volume 5A: 43rd Mechanisms and Robotics Conference*. Anaheim, California, USA: American Society of Mechanical Engineers, Aug. 2019.

[14] A. El Magri, K. El Mabrouk, S. Vaudreuil, and M. Touhami, "Mechanical properties of CF-reinforced PLA parts manufactured by fused deposition modeling," *Journal of Thermoplastic Composite Materials*, vol. 32, May 2019.

[15] X. Gao, Y. Liu, S. Zhang, J. Deng, and J. Liu, "Development of a Novel Flexure-Based XY Platform Using Single Bending Hybrid Piezoelectric Actuator," *IEEE/ASME Transactions on Mechatronics*, pp. 1–11, 2022.

[16] Q. Xu, "Design and Development of a Compact Flexure-Based XY Precision Positioning System With Centimeter Range," *IEEE Transactions on Industrial Electronics*, vol. 61, no. 2, pp. 893–903, Feb. 2014.